ADVANCING EARTH AND SPACE SCIENCES

Geophysical Research Letters

RESEARCH LETTER
10.1029/2026GL122792

# Unprecedented Wetting Over Western Central Asia Dominated by Internal Climate Variability

**Yu Ren[1], Jianping Huang[2], Haipeng Yu[3], Xiaolu Fan[1], Kangjie Ma[1], Xin Wang[4], Yongqi Gong[1], Yihui Xu[1], and Jinxia Zhang[1]**

[1]College of Atmospheric Sciences, Lanzhou University, Lanzhou, China, [2]Collaborative Innovation Center for Western Ecological Safety, Lanzhou University, Lanzhou, China, [3]State Key Laboratory of Cryospheric Science and Frozen Soil Engineering, Nagqu Plateau Climate and Environment Observation and Research Station of Tibet Autonomous Region, Northwest Institute of Eco-Environment and Resources, Chinese Academy of Sciences, Lanzhou, China, [4]College of Earth and Environmental Sciences, Lanzhou University, Lanzhou, China

**Key Points:**

- An abrupt and unprecedented wetting during 1988–2007 is dominated by the internal variability rather than external forcing
- The negative-to-positive phase transition of mid-high-latitude North Atlantic sea-surface temperature (NAS) explains 45% of observed wetting
- Accounting for NAS-related variability reduces precipitation projection uncertainty by 28.39% for near-future periods

**Supporting Information:**

Supporting Information may be found in the online version of this article.

**Correspondence to:**

J. Huang,
hjp@lzu.edu.cn

**Citation:**

Ren, Y., Huang, J., Yu, H., Fan, X., Ma, K., Wang, X., et al. (2026). Unprecedented wetting over western central Asia dominated by internal climate variability. *Geophysical Research Letters*, *53*, e2026GL122792. https://doi.org/10.1029/2026GL122792

Received 4 MAR 2026
Accepted 23 JUN 2026

**Author Contributions:**

**Conceptualization:** Jianping Huang, Haipeng Yu
**Data curation:** Yongqi Gong, Jinxia Zhang
**Formal analysis:** Yu Ren, Jianping Huang, Haipeng Yu, Xiaolu Fan, Yongqi Gong
**Investigation:** Jianping Huang, Kangjie Ma, Xin Wang
**Methodology:** Yu Ren, Xiaolu Fan, Kangjie Ma, Xin Wang



**Abstract** Spring precipitation over western Central Asia (SCAP) experienced an abrupt and unprecedented wetting during 1988–2007, yet the relative contributions of external forcing and internal variability to this change and the underlying drivers remain unclear. Using observation data sets and large ensemble simulations, our study demonstrates that this wetting is dominated by internal climate variability. Specifically, mid-high-latitude North Atlantic sea-surface temperature (NAS) variability drives interdecadal SCAP changes by exciting a Eurasian Rossby wave train, which enhances ascent motion over western Central Asia and promotes moisture transport into the region. A negative-to-positive NAS phase transition explains 44.82% of the 1988–2007 wetting, far exceeding the externally forced contribution (21.72%). Under mid-intensity emission scenario, removing NAS-related rainfall variability reduces near-term SCAP projection uncertainty by 28.39%, highlighting NAS as a key source of predictability for hydroclimate risk on western Central Asia.

**Plain Language Summary** Spring precipitation over western Central Asia (SCAP) is critical for agriculture, water resources, and ecological resilience. The region experienced exceptional springtime wetting during 1988–2007 that was abrupt and unusual in the historical record. Both external forcing and internal variability play important roles in the precipitation variability, but their relative contributions to the wetting are still unknown. Using observations together with large ensemble simulations, we identify that the internal variability dominates the significant increase in SCAP. Among the internally components, mid-high-latitude North Atlantic sea-surface temperature (NAS) variability is identified as the primary driver, with NAS warming triggering a robust Eurasian Rossby wave train. Western Central Asia lies to the southeast of the associated anomalous cyclone, leading to enhanced ascent motion and strengthened anomalous southwesterly and northwesterly moisture transport, thereby increasing precipitation over the region. A negative-to-positive phase transition of the NAS explains 44.82% of the observed wetting during 1988–2007, much greater than the role of external forcing (21.72%). Under mid-intensity emission scenario, removing the influence of the NAS can reduce near-term projection uncertainty for SCAP by 28.39%, which is important for constraining projection of SCAP.

## 1. Introduction

Western Central Asia (42°–55°N, 40°–65°E) is an inland region situated at the intersection of Europe and Asia, characterized by arid to semi-arid climates and encompassing Turkmenistan, Uzbekistan, Tajikistan, Kazakhstan, and parts of eastern Europe (Mariotti, 2007). The region features arid highlands, deserts, and vast steppes, where water resources are highly sensitive to climate change (Aizen et al., 2001; Chen et al., 2011; Huang et al., 2013). Rain-fed agriculture is the primary agricultural system, rendering the region strongly dependent on precipitation (Zou et al., 2020). Precipitation is mainly controlled by mid-latitude westerly disturbances and exhibits pronounced seasonality (Chen et al., 2008; Peng et al., 2020; Wang et al., 2022). Among all seasons, spring precipitation over western Central Asia (SCAP) is especially consequential for livestock, agriculture, and regional socio-economic stability (Jiang & Zhou, 2023; Yao, Tang, & Huang, 2024, Yao, Tang, Huang, & Wu, 2024). For example, precipitation deficits during the spring 2021 agricultural drought caused widespread forage shortages and the death of thousands of sheep, cattle, and horses across Central Asia (Guo et al., 2024). In late March–April 2024, the most severe flooding in past 70 years struck large areas of Kazakhstan and southwestern Russia, causing widespread devastation (Zhang et al., 2025).

**Resources:** Yihui Xu
**Software:** Yu Ren
**Visualization:** Yihui Xu, Jinxia Zhang
**Writing – original draft:** Yu Ren, Haipeng Yu, Xiaolu Fan
**Writing – review & editing:** Yu Ren, Jianping Huang

Over the past 80 years, SCAP has exhibited a fluctuating increasing trend (Chen et al., 2011; Yan & Zhao, 2022), with particularly pronounced and accelerated wetting observed during 1988–2007 (Figure 1a). Consistently, extreme precipitation has intensified since the late 1980s: very-wet-day precipitation increased from 36.64 mm before 1986 to 47.84 mm after 1986, while its trend accelerated from 0.8 to 5.06 mm decade$^{-1}$ (Wei et al., 2023). The mechanisms driving Central Asian precipitation changes are complex, containing both external forced responses and internal variability (Hoell et al., 2015; Jiang et al., 2021). Anthropogenic forcing can increase the likelihood of extreme precipitation over Central Asia, with changes of about 100% in intensity and 20% in frequency (Fallah et al., 2024; Fallah & Rostami, 2024). Greenhouse gas (GHG) emissions favor an equatorial shift of Subtropical Westerly Jet (SWJ) and increased summer precipitation over Northern Central Asia; whereas aerosol emissions generally weaken the SWJ and suppress summer precipitation there (Jiang & Zhou, 2021); similar phenomena of GHG and anthropogenic aerosols forcing the regulation of westerly jets to affect precipitation also occurs in winter (Yao et al., 2025). Internal precipitation variability over Central Asia is influenced by various climate modes. At interdecadal and multidecadal timescales, Pacific and Atlantic Surface Sea Temperature (SST) variability can exert far-reaching influences on regional hydroclimate (Umirbekov et al., 2022). For example, the positive-to-negative phase transition of the Interdecadal Pacific Oscillation around 1992 is associated with aggravated agricultural drought in Central Asia (Jiang & Zhou, 2023). The associated tropical Pacific decadal variability can influence Central Asia through moisture transport changes related to Indo–western Pacific pressure anomalies and Rossby wave trains forced by enhanced tropical Pacific convection (Barlow et al., 2016; Hoell et al., 2015; Jiang et al., 2021; Mariotti, 2007). North Atlantic SST anomalies also play a crucial role in influencing Eurasian climate anomalies (Chen et al., 2022; Cheng et al., 2024; Monerie et al., 2021). Positive SST anomalies over the North Atlantic, especially its northern part, can trigger an eastward zonal wave train located along the Northern Hemisphere westerly jet (Jiang et al., 2021; Ren et al., 2022, 2025; Xie et al., 2021), influencing the dry and wet changes over East Europe and Central Asia. When the Central Asia is controlled by an anomalous cyclone, strengthened westerlies along the cyclone's southern flank transport moisture from the North Atlantic and northern Europe into northern Central Asia, increasing precipitation (Jiang et al., 2021). Despite these advances, the extent to which these mechanisms drove the rapid 1988–2007 wetting has not been quantitatively assessed, and the relative contribution of internal variability versus external forcing remains largely unknown.

Our study utilizes a 100-member Community Earth System Model v2 Large Ensemble (CESM2-LENS) to explore the causes of the pronounced 1988–2007 wetting over western Central Asia. Two key questions are addressed: (a) to what extent did internal climate variability drive the 1988–2007 wetting? and (b) how does this internally driven decadal signal influence the uncertainty in near-term precipitation projections before 2044? Answering these questions provides new insights into the decadal hydroclimate evolution and prediction of western Central Asia.

## 2. Methods and Data

### 2.1. Observations and Reanalysis Data

Monthly atmospheric fields are obtained from the Japanese 55-year Reanalysis (JRA-55) for 1958–2024, including geopotential height, air temperature, vertical velocity, and zonal and meridional winds. Three monthly gridded precipitation data sets are used: (a) the Met Office Hadley Center gridded land surface extremes indices (HadEX3) for 1901–2018; (b) the Climatic Research Unit Time Series version 4.09 (CRU TS v4.09) for 1901–2024; and (c) the Global Precipitation Climatology Center (GPCC) Full Data Reanalysis, full 2020 version, for 1891–2019. Monthly SST data are obtained from the NOAA/NCEI Extended Reconstructed SST, version 6, for 1854–2024. Trend significance is assessed using the Mann–Kendall test and a non-parametric bootstrap approach.

### 2.2. Model Simulations

Two 100-member large ensembles are analyzed: the MPI Grand Ensemble (MPI-GE) and CESM2-LENS. Monthly precipitation, SST, and geopotential height are examined. For CESM2-LENS, historical (1961–2014) and Shared Socio-economic Pathways 3–7.0 (2015–2024) emission scenario simulations are concatenated to form a continuous 1961–2024 series consistent with the observations. The near-term projection period is defined

10.1029/2026GL122792

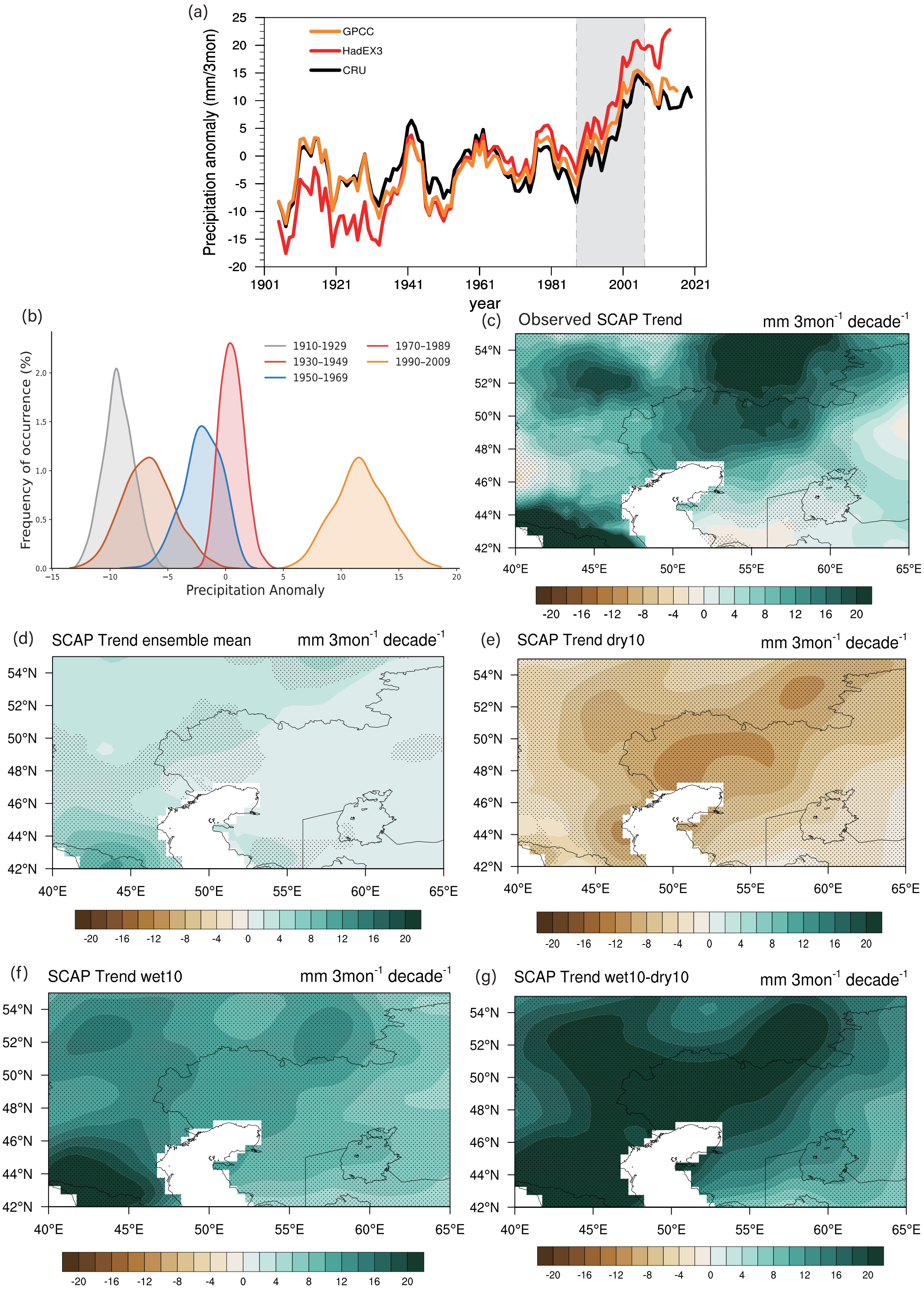


**Figure 1.** Observed and simulated SCAP trends during 1988–2007. (a) 9-year running-mean SCAP anomalies averaged over 42°–55°N, 40°–65°E from CRU, HadEX3, and Global Precipitation Climatology Center. (b) Distributions of 20-year mean SCAP anomalies (relative to 1961–2010) for 20-year windows from 1910 to 2009 based on HadEX3, estimated using a block bootstrap. (c) Observed SCAP trends in 1988–2007. (d) CESM2-LENS ensemble-mean trends. (e)–(g) As in (c), but for (e) dry10 sub-ensemble mean, (f) wet10 sub-ensemble mean, and (g) wet10 minus dry10. Stippling denotes trends significant at 5% level.

as 2025–2044 under SSP3–7.0 Scenario. MPI-GE historical simulations are used for evaluation and comparison to enhance robustness, and 2000-year CESM2 pre-industrial (PI) control run are used to further sample internal variability and corroborate the mechanisms identified from observations and large ensembles.

### 2.3. Separation of External Forcing and Internal Variability

A 9-year running mean is applied to all monthly observational and model fields, except SST, to extract decadal variability. For a climate variable $X$, all ensemble members are driven by same external forcing; therefore, the ensemble mean represents the externally forced response:

$$X_{\text{external}} = (X(i))_{EM}, \qquad i = 1, 2, \ldots, 100 \tag{1}$$

and deviations from the ensemble mean are interpreted as internal variability:

$$X(i) = X_{\text{external}} + X_{\text{internal}}(i), \qquad i = 1, 2, \ldots, 100 \tag{2}$$

### 2.4. Definition of the NAS Index

The NAS index is defined as the 13-year running mean of spring SST anomalies averaged over the mid-high-latitude North Atlantic (60°W–10°E, 47°N–70°N), after removing the global-mean SST anomaly. For each ensemble member $i$, NAS$(i, t)$ is computed by applying a 13-year running mean to the area-averaged spring-mean $\text{SST}_{\text{internal}}(i)$ anomalies in the same area. Additionally, the NAS index is also calculated by subtracting the CESM2-LENS ensemble-mean SST. This definition is highly consistent with the global-mean-removal NAS index ($r = 0.953$, $p < 0.01$), although its amplitude is slightly weaker (Figure S1 in Supporting Information S1).

### 2.5. Adjustment of SCAP Based on Observational NAS

Following a large-ensemble-based phase-alignment approach (Huang et al., 2020; Jiang & Zhou, 2023; Liu et al., 2024; Zhang et al., 2024), we quantify the NAS contribution to SCAP trends by replacing each member's simulated NAS-related precipitation trend with that implied by the observed NAS evolution. For member $i$, the adjusted trend is:

$$\frac{\partial P_{\text{adj}}(i)}{\partial t} = \frac{\partial P_{\text{external}}}{\partial t} + \frac{\partial P_{\text{internal-adj}}(i)}{\partial t}, \qquad i = 1, 2, \ldots, n-1, n \tag{3}$$

where $\frac{\partial P_{\text{external}}}{\partial t}$ is the externally forced SCAP trend during 1988–2007. The adjusted internally generated component is:

$$\frac{\partial P_{\text{internal-adj}}(i)}{\partial t} = \frac{\partial P_{\text{internal}}(i)}{\partial t} + r_{P,\text{NAS}}(i) \cdot \left( \frac{\partial \text{NAS}_{\text{obs}}}{\partial t} - \frac{\partial \text{NAS}(i)}{\partial t} \right) \tag{4}$$

Where $\frac{\partial P_{\text{internal}}(i)}{\partial t}$ is the internally driven SCAP change in member $i$ before the NAS phase adjustment, and $r_{P,\text{NAS}}(i)$ is the regression coefficient of SCAP regressed onto the NAS index in member $i$. The term $r_{P,\text{NAS}}(i) \cdot \frac{\partial \text{NAS}_{\text{obs}}}{\partial t}$ represents the SCAP trend induced by the observed NAS evolution, whereas $r_{P,\text{NAS}}(i) \cdot \frac{\partial \text{NAS}(i)}{\partial t}$ represents the NAS-related SCAP trend in member $i$. After ensemble averaging $\frac{\partial P_{\text{internal-adj}}(i)}{\partial t}$, NAS-unrelated internal variability is largely canceled across members, leaving the SCAP trend attributable to the observed NAS phase evolution. Similarly, the ensemble mean of $\frac{\partial P_{\text{adj}}(i)}{\partial t}$ represents the combined effect of external forcing and the observed NAS-related internal component.

### 2.6. Removing NAS's Influence

To quantify the NAS contribution to the spread of near-term SCAP projections, the NAS-related component is removed from each member's projected SCAP trend during 2025–2044:

$$\frac{\partial P_{\text{non-NAS}}(i)}{\partial t} = \frac{\partial P(i)}{\partial t} - r_{P,\text{NAS}}(i)\frac{\partial \text{NAS}(i)}{\partial t}, \qquad i = 1, 2, \ldots, 100 \tag{5}$$

where $\frac{\partial P_{\text{non-NAS}}(i)}{\partial t}$ is the SCAP trend after removing NAS influence in member $i$, $\frac{\partial \text{NAS}(i)}{\partial t}$ is the NAS trend during 2025–2044, and $r_{P,\text{NAS}}(i)$ is the regression coefficient of SCAP regressed onto the NAS index during 2025–2044. The term $r_{P,\text{NAS}}(i)\frac{\partial \text{NAS}(i)}{\partial t}$ denotes the NAS-induced precipitation trend. Comparing ensemble spread before and after removing the NAS contribution can quantify the extent to which NAS-related variability contributes to near-term projection uncertainty.

### 2.7. Block Bootstrap Method

The bootstrap method is a nonparametric approach for estimating the sampling distribution of a statistic through repeated resampling from the original data set (Austin & Tu, 2004). The block bootstrap extends this method to data with serial dependence, such as time series. For the SCAP time series, five 20-year subsets spanning 1910–2009 were first selected, and a block bootstrap was then applied to each subset. In each resampling step, a consecutive 3-year block was randomly drawn from the original subset, with overlapping blocks allowed. The selected blocks were concatenated until the bootstrap sample reached the same length as the original subset, helping preserve the distributional characteristics of the original record. This procedure was repeated 1,000 times for each subset, and the mean SCAP anomaly is calculated for each bootstrap sample, yielding 1,000 resampled means. The histogram of SCAP anomalies was then constructed from the 1,000 resampled means, providing a more realistic estimate of distribution of the sample mean.

## 3. Results

### 3.1. Internal Variability Dominates Strong Wetting in Western Central Asia

Multiple gridded observational data sets consistently show that SCAP experienced an abrupt and exceptionally strong increase during 1988–2007, with an average trend of 10.91 (10.12 ~ 11.84) mm 3 mon$^{-1}$ decade$^{-1}$ ($p < 0.05$) (Figure 1a). This wetting was mainly concentrated over northwestern Central Asia and the southwestern part of the domain (Figure 1c). Using HadEX3, five 20-year subsets from 1910 to 2009 were selected, and SCAP anomalies were resampled 1000 times to construct their distributions (Figure 1b). The distributions before 1990 are tightly clustered, whereas the post-1990 distribution lies entirely outside the previous range, indicating that post-1990 SCAP was unprecedented and statistically distinct from those before 1990.

SCAP variability is decomposed using the 100-member CESM2-LENS, with the ensemble mean representing the externally forced response and inter-member deviations representing internal variability (Deser et al., 2012; Rodgers et al., 2021). The ensemble mean realistically reproduces the climatology of SCAP (Figure S2 in Supporting Information S1). The externally forced trend over western Central Asia is weak, amounting to 2.37 mm 3 mon$^{-1}$ decade$^{-1}$ and explaining only 21.72% of the observed increase (Figures 1c and 1d). Long-term SST warming driven by external forcing induces an anomalous anticyclone over southwestern Asia, enhancing moisture transport from the northern Indian Ocean into western Central Asia (Hoell et al., 2015). In contrast, internally generated rainfall trends span −13.48 to +18.00 mm 3 mon$^{-1}$ decade$^{-1}$, fully encompassing the observed wetting (Figure S3 in Supporting Information S1).

To further explore the impact of internal climate variability, we examine two sub-ensembles comprising the 10 wettest and 10 driest members, hereafter wet 10 and dry 10. The wet 10 sub-ensemble produces pronounced wetting over western Central Asia, with a mean trend of +11.06 mm 3 mon$^{-1}$ decade$^{-1}$, comparable to observations (Figures 1a and 1f). In contrast, the dry 10 sub-ensemble exhibits significant drying of −6.64 mm 3 mon$^{-1}$ decade$^{-1}$ (Figure 1e). The wet 10–dry 10 composite trends reproduces the spatial pattern of the observed SCAP trend (Figure 1g), underscoring the dominant role of internal climate variability in driving the abrupt 1988–2007 wetting.

### 3.2. Influence Mechanism of NAS for Internal Variability of SCAP

To identify which internal variability dominates the SCAP decadal variability, empirical orthogonal function analysis is performed to the observed SCAP during 1961–2024. The leading mode (EOF1) explains 65.1% of the

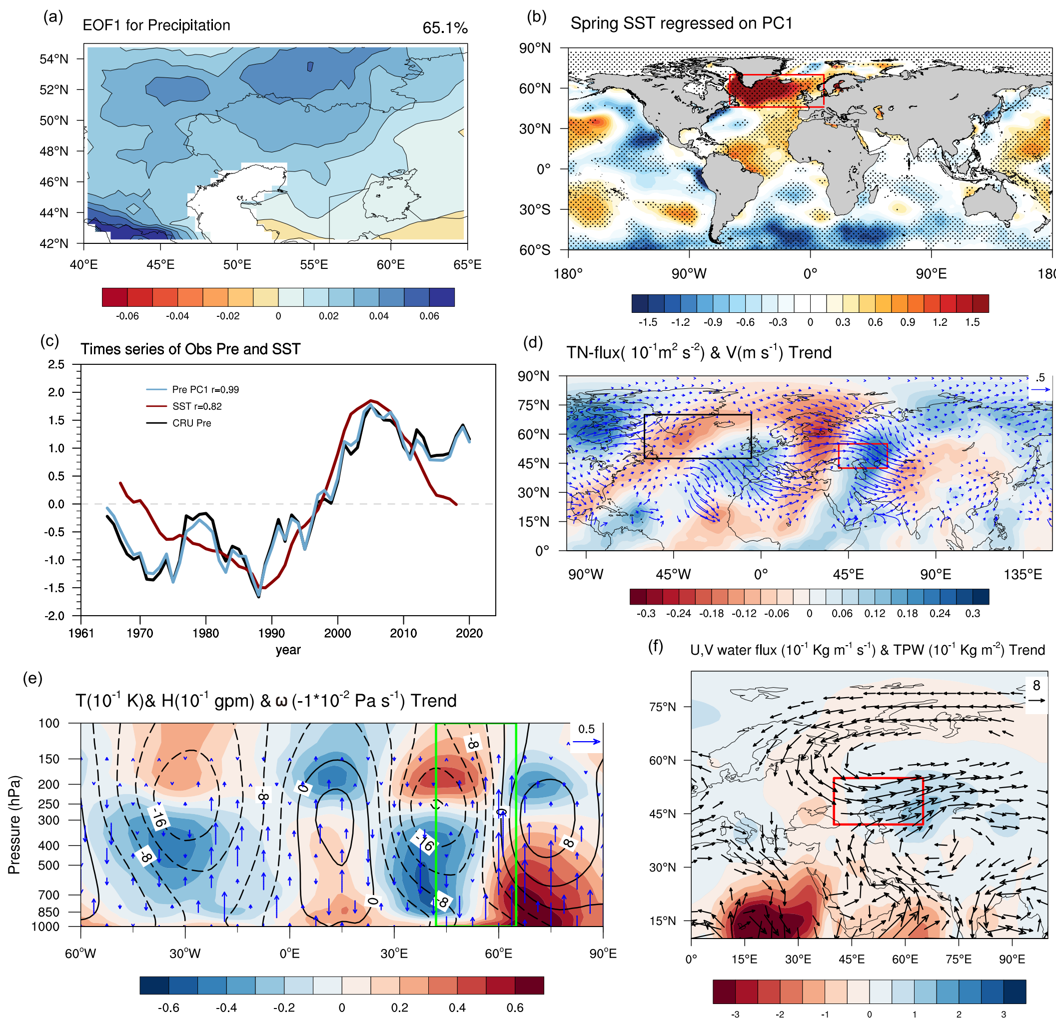


**Figure 2.** Leading mode of SCAP variability and associated Surface Sea Temperature (SST) and circulation patterns. (a) EOF1 of 9-year running-mean SCAP from CRU. (b) Global detrended spring SST regressed onto PC1 (1961–2024); Stippling denotes regression significant at the 5% level, and the red box marks the NAS region. (c) Normalized PC1 (blue), area-averaged SCAP anomalies (black), and NAS index (red). (d) Spring trends (1988–2007) of 250-hPa Takaya–Nakamura wave activity flux (vectors; $10^{-1}$ m$^2$ s$^{-2}$) and meridional wind (shading; m s$^{-1}$). (e) Longitude–height section (42°–55°N mean) of spring trends in air temperature (shading; $10^{-1}$ K), geopotential height (contours; $10^{-1}$ gpm), and vertical velocity (arrows; $-10^{-2}$ Pa s$^{-1}$). (f) As in (d), but for spring vertically integrated water-vapor flux (vectors; $10^{-1}$ kg m$^{-1}$ s$^{-1}$) and precipitable water (shading; $10^{-1}$ kg m$^{-2}$).

total variance and exhibits a largely consistent spatial pattern across western Central Asia, except for localized deviations in the southeast (Figure 2a). To explore the influence of ocean variability on SCAP, regressing detrended global spring SST anomalies onto the corresponding principal component (PC1) reveals a pronounced warming over the mid-high-latitude North Atlantic (47°–70°N, 60°W–10°E; Figure 2b). The NAS index exhibits a strong temporal correlation with PC1 ($r = 0.82$; Figure 2c), indicating that mid-high-latitude North Atlantic SST variability is tightly linked to the dominant mode of SCAP interdecadal variations.

Focusing on the period 1988–2007, this mid-high-latitude North Atlantic SST anomaly excites an eastward-propagating Rossby wave train across the Eurasian mid-latitudes (Figure 2d), producing alternating geopotential height anomalies. Western Central Asia lies in the trough–ridge transition zone, accompanied by a barotropic pressure structure and large-scale ascending motion (Figure 2e). Correspondingly, two moisture transport pathways are identified: (a) an anomalous cyclone over northern Central Asia that bring northwesterly moisture from the Arctic Ocean into western Central Asia, and (b) an anomalous anticyclone located in the southeast of western Central Asia that transports moisture from the northern Indian Ocean and Arabian Sea

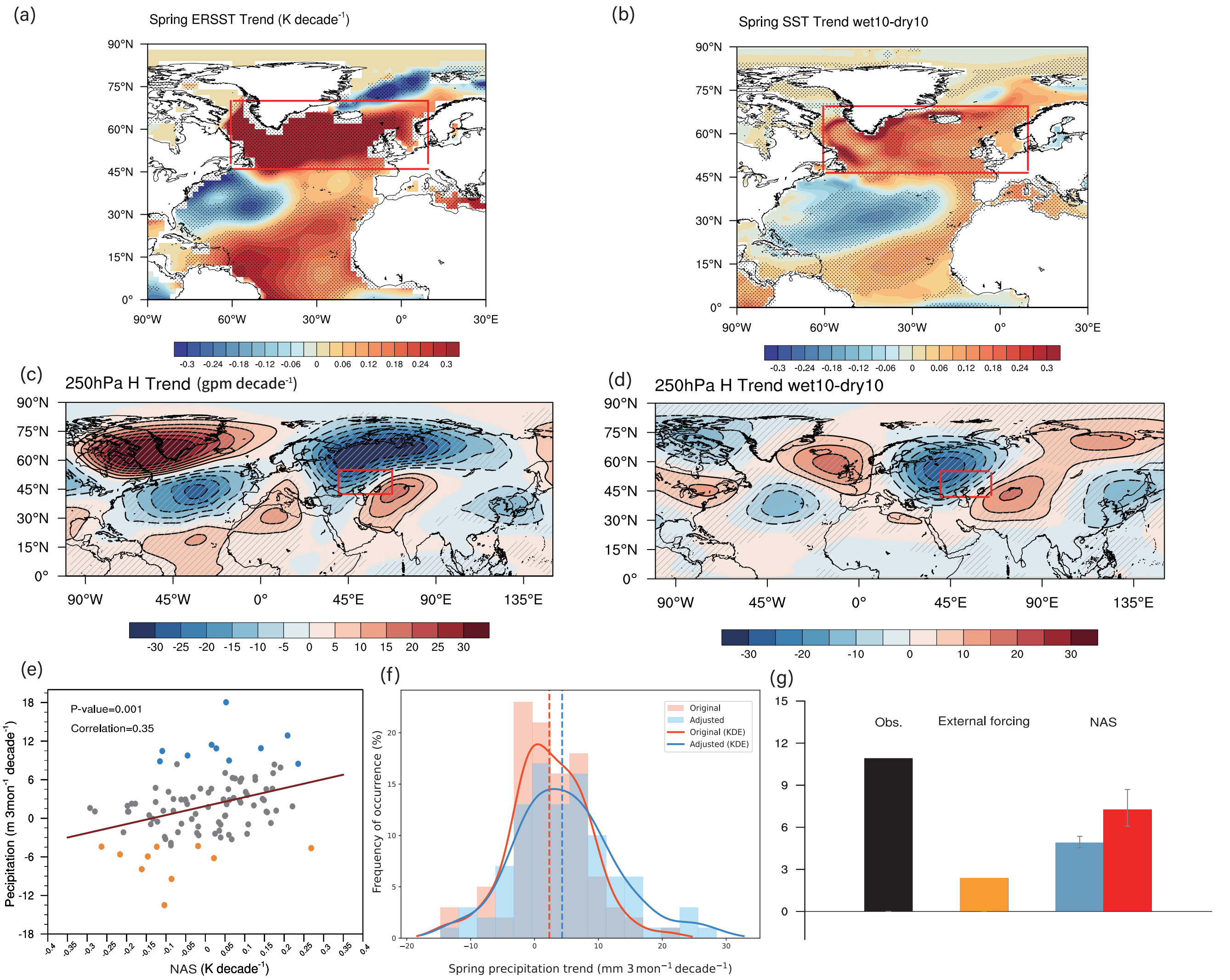


**Figure 3.** NAS contributions to the observed SCAP trend (1988–2007). (a) Spring Surface Sea Temperature (SST) trends from ERSST (K decade$^{-1}$). (b) Wet10–dry10 composite difference in spring SST trends (K decade$^{-1}$). (c) As in (a), but for observed 250-hPa geopotential height trends (gpm decade$^{-1}$). (d) As in (b), but for 250-hPa geopotential height trends (gpm decade$^{-1}$). Stippling and shading denote trends significant at the 5% level. (e) NAS index trends (K decade$^{-1}$) versus SCAP trends (mm 3mon$^{-1}$ decade$^{-1}$) across 100 CESM2-LENS members; blue/orange denote wet10/dry10. (f) Distributions of SCAP trends for the original (orange) and NAS-phase-adjusted (blue) simulations; vertical lines mark ensemble means. (g) Observed (average of CRU, HadEX3, and GPCC, black), externally forced (yellow), and NAS-related contributions (blue) to the 1988–2007 SCAP trend; red shows the total after NAS phase alignment. Error bars show 5th–95th bootstrapped percentiles of ensemble-mean trends.

toward western Central Asia along its southwestern flank (Figure 2f). Moreover, NAS-regressed precipitation reproduces the EOF1 pattern (Figure S4a in Supporting Information S1), and NAS-regressed Takaya–Nakamura wave activity flux and meridional wind anomalies show spatial patterns consistent with the directly calculated 1988–2007 trends (Figure 2d; Figure S4c in Supporting Information S1), further confirming the role of North Atlantic SST in modulating SCAP at interdecadal timescales.

We further investigate whether the observed NAS-related circulation anomalies are reproduced when internal variability is isolated in CESM2-LENS. The wet 10-dry 10 composite SST trend demonstrates pronounced warming over the mid-high-latitude North Atlantic (Figure 3b), in close agreement with observations (Figure 3a). Consistently, the wet 10-dry 10 250-hPa geopotential height trend also resembles the observed structure, with a significant pattern correlation of 0.58 ($p < 0.01$) over 30°–75°N, 60°W–90°E; western Central Asia lies between an upper-level trough to the northwest and a ridge to the southeast (Figures 3c and 3d). CESM2-LENS captures a reasonable connection between the NAS and SCAP (Figure S5 in Supporting Information S1). Across 100 members, NAS changes are significantly positively correlated with SCAP changes ($r = 0.35$; $p < 0.01$; Figure 3e). The EOF1 of intermember spring rainfall trend over western Central Asia explains 40.6% of the total variance; and SST trends regressed onto the corresponding PC1 show significant positive anomalies over the mid-high-latitude North Atlantic (Figure S6 in Supporting Information S1), further supporting North Atlantic SST as a leading source of member-to-member SCAP differences.

The 2000-year CESM2 PI control run provides further evidence. We calculate the 13-year running SCAP trends and identify the 10 slices with the strongest wetting (drying) 20-year trend, referred to as PI wet 10 and PI dry 10, respectively (Figure S7a in Supporting Information S1). The center years of these slices are separated by more than 20 years to avoid overlap. The SST difference between PI wet 10 and PI dry 10 exhibits mid-high-latitude North Atlantic warming (Figure S7d in Supporting Information S1). Consistently, the difference in spring 250-hPa geopotential height between PI wet 10 and PI dry 10 shows a clear wave train across the Northern Hemisphere mid-high latitudes, accompanied by a cyclonic anomaly over the western Central Asia (Figure S7c in Supporting Information S1), in close agreement with the observational results (Figure 3c). Additionally, we analyze the MPI-GE large-ensemble simulations to strengthen the robustness of our conclusions, which consistently show a similar warming trend over the mid-high-latitude North Atlantic (Figure S8a in Supporting Information S1). Across wet10 and dry10 members selected from MPI-GE, CESM2-LENS, and the CESM2 PI control run, SCAP trends are significantly and positively correlated with NAS trends ($r = 0.38$, $p < 0.05$; Figure S8b in Supporting Information S1).

To explicitly quantify the contribution of NAS variability to the 1988–2007 wetting, the NAS evolution has been adjusted in CESM2-LENS simulations. For each ensemble member, we first remove the member-simulated NAS-related SCAP component and then add the observed NAS-related SCAP signal, estimated by regressing SCAP onto NAS during 1988–2007. This adjustment replaces each member's random NAS evolution with the observed NAS phase transition, enabling the isolation of NAS contribution to the observed wetting. The adjusted SCAP change therefore reflects the combined effects of external forcing and the observed NAS transition. Before adjustment, 63% of the ensemble members can simulate an increasing SCAP trend during 1988–2007, whereas after the adjustment this proportion rises to 71% (Figure 3f). The ensemble mean of the adjusted SCAP increase is 7.26 (6.09 ~ 8.62) mm 3 $\text{mon}^{-1}$ $\text{decade}^{-1}$, accounting for approximately 66.54% (55.82 ~ 79.01%) of the observed change; the ensemble mean NAS-induced increase in SCAP is 4.89 (4.53 ~ 5.35) mm 3 $\text{mon}^{-1}$ $\text{decade}^{-1}$, accounting for 44.82% (41.52 ~ 49.04%) of the observed change, substantially exceeding the externally forced contribution (Figure 3g).

### 3.3. Influence of NAS on Near-Term SCAP Projection Uncertainty

Given the strong influence of NAS on interdecadal SCAP variability, we assess whether NAS phase transition also influence the near-term projection of SCAP change. Under the SSP3–7.0 Scenario, the CESM2-LENS ensemble mean displays a sustained increase in SCAP in the 21st century, consistent with previous studies (Fallah et al., 2024; Jiang et al., 2020). However, substantial uncertainty from internal variability persists among different members. Across all 100 members, area-averaged SCAP trends during 2025–2044 exhibit a wide spread, ranging from −10.37 to +14.43 mm 3 $\text{mon}^{-1}$ $\text{decade}^{-1}$ (Figure 4d). We also take the sub-ensembles of 10 members with wettest and driest rainfall trends over the period of 2025–2044. The wet 10-dry 10 composite rainfall trends are large and far exceeds the externally forced trend (Figures 4a and 4c).

To assess whether part of the near-term projection uncertainty originates from the NAS, we examine the spatial pattern of SST trends during 2025–2044. The difference of SST trends between wet 10 and dry 10 reveals a positive-NAS-like pattern with warming in the mid-high-latitude North Atlantic (Figure 4b). Regressing the projected grid-point rainfall and SST trends against projected SCAP trend during 2025–2044 for the inter-members, the results indicate that there is a prominent positively rainfall anomaly center over the western Central Asia, in association with the positive NAS-like pattern (Figure S9 in Supporting Information S1). Thus, the NAS phase evolution constitutes an important source of uncertainty in near-term SCAP projections. To quantify its contribution to the spread of projected SCAP trends, we remove the NAS's influence from each member by subtracting the SCAP variations linearly associated with the NAS, from each member during 2025–2044. Therefore, the rest of the rainfall trend is can be attributed to external forcing and other internal variability. After removing the NAS influence, the spread across all members is reduced by 28.39%, from −10.37

10.1029/2026GL122792

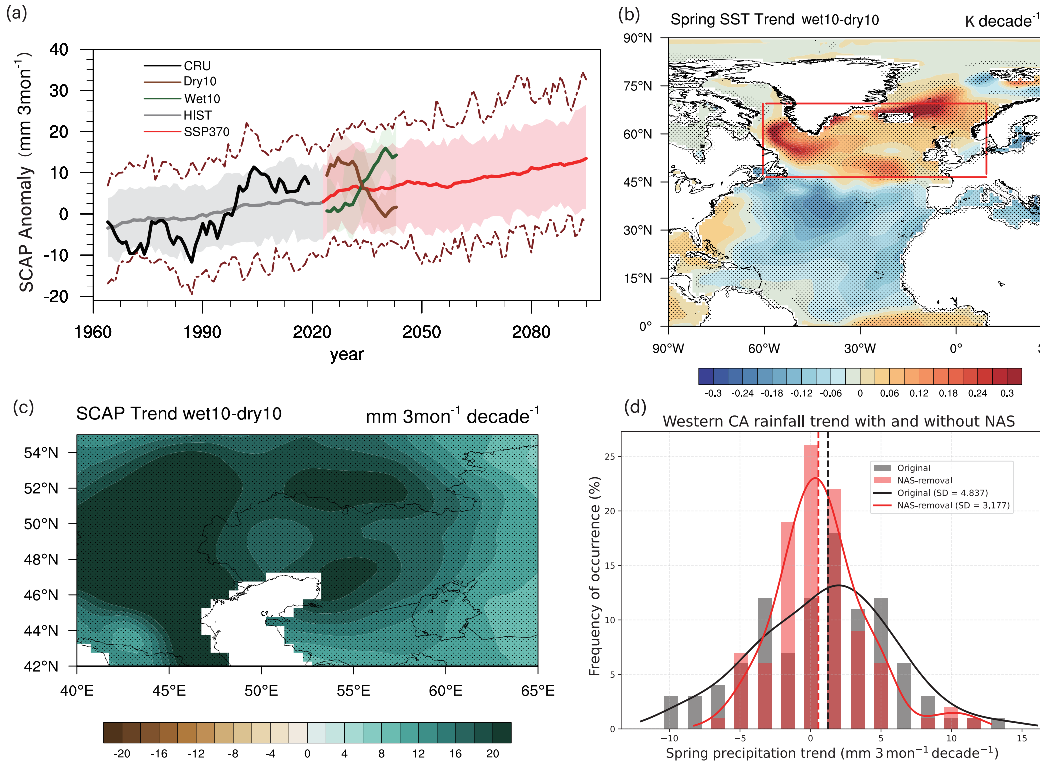


**Figure 4.** Near-term SCAP projections and associated Surface Sea Temperature (SST) changes. (a) 9-year running-mean SCAP anomalies from CRU (1961–2024; black) and CESM2-LENS (historical: gray; SSP3–7.0: red), showing the 5th–95th percentile range (shading), ensemble mean (thick), maximum and minimum (dashed). Wet10 and dry10 (selected by 2025–2044 SCAP trends) are shown by green and brown lines with their 5th–95th ranges (green and brown shading). (b)–(c) Wet–dry10 trend during 2025–2044 for (b) spring SST and (c) SCAP. Stippling denotes trends significant at the 5% level. (d) Distributions of area-averaged SCAP trends (2025–2044) across 100 members for the original simulations (gray/black) and after removing the NAS-related component (orange/red).

to +14.43 mm 3 mon$^{-1}$ decade$^{-1}$ to −6.60 to +11.16 mm 3 mon$^{-1}$ decade$^{-1}$. Meanwhile, the intermember standard deviation decreased by 34.30%, from 4.84 to 3.18 mm 3 mon$^{-1}$ decade$^{-1}$.

## 4. Conclusions and Discussion

In this study, we identify a pronounced decadal-scale spring wetting over western Central Asia during 1988–2007 and show, using large-ensemble simulations, that it is dominated by internal variability associated with a phase transition of NAS. NAS warming excites an eastward-propagating Eurasian Rossby wave train, with an anomalous cyclone northwest of Central Asia that enhances ascent motion and moisture transport from the Arctic and the Arabian Sea. The negative-to-positive NAS transition explains 44.82% of the observed SCAP increase, far exceeding the externally forced contribution (21.72%). NAS-related variability also contributes substantially to near-term projection uncertainty, which is reduced by 28.39% after removing the NAS signal. These results highlight NAS as a key source of predictability for hydroclimate risk in this climate-change hotspot. Future work should explore constrained near-term SCAP projections by NAS phase evolution.

Recent large-ensemble attribution studies have also highlighted the importance of North Atlantic SST variability in shaping regional hydroclimate changes. For example, Li et al. (2024) used initial-condition large ensembles and dynamical adjustment to attribute recent drought trends over the Mongolian Plateau, showing that internally generated interdecadal warming of mid-high-latitude North Atlantic SST triggers a zonally oriented atmospheric wave train and accounts for approximately 57% of the regional drought trend. Similarly, Si et al. (2025) showed, using large-ensemble all-forcing and North Atlantic pacemaker experiments, that North Atlantic cooling modulates weakened the East Asian summer monsoon in the late 1960s through a mid-latitude Rossby wave train and an equatorial Kelvin wave.

Expect SST driven variability, atmospheric internal variability also shapes Central Asian precipitation. For example, storm activity is significantly negatively correlated with the summer North Atlantic Oscillation; the recent shift toward its negative phase has displaced storm tracks southward, allowing more extratropical storms to enter southeastern Central Asia and enhance summer precipitation (Dong et al., 2024). For cold-season precipitation, the concurrent positive phases of the Arctic Oscillation and the East Atlantic/Western Russia pattern favor weather types featuring a Rossby trough over Central Asia, strengthening westerly moisture fluxes (Gerlitz et al., 2018, 2019). Under the SSP5–8.5 scenario, projection uncertainty in Central Asian precipitation is dominated by the dynamic component of vertical moisture transport, with enhanced ascent linked to out-of-phase variations between the two Eurasian westerly jets (Yao, Tang, & Huang, 2024, Yao, Tang, Huang, & Wu, 2024).

Although the externally forced SCAP trend is weaker than the NAS-related internally generated component in our analysis, external forcing may still modulate the precipitation response by altering the background hydroclimatic state. GHG-induced warming increases atmospheric moisture capacity and intensifies the hydrological cycle, providing a favorable thermodynamic background for precipitation increases (Donat et al., 2016; Held & Soden, 2006; Oki & Kanae, 2006). Over Central Asia, the 1979–2014 increase in winter precipitation has been shown to be largely controlled by this thermodynamic moistening effect (Guo et al., 2026). Beyond GHG forcing, Asian sulfate aerosols can enhance summer precipitation by modulating the westerly jet and strengthening moisture transport into Central Asia (Guo et al., 2026). The impacts of atmospheric internal variability and external forcing merit further investigation in future work.

## Conflict of Interest

The authors declare no conflicts of interest relevant to this study.

## Availability Statement

Data related to the paper can be downloaded from the following: CRU v4.09 at https://crudata.uea.ac.uk/cru/data/hrg/cru_ts_4.09/; GPCC data are available at Schneider et al. (2020); HadEX3 precipitation at https://www.metoffice.gov.uk/hadobs/hadex3/index.html; JRA-55 data can be found from Japan Meteorological Agency/Japan (2013); CESM2-LENS at https://www.cesm.ucar.edu/community-projects/lens2; CESM2 PI control at https://www.cesm.ucar.edu/working-groups/climate/simulations/cam6-picontrol; ERSST V6 at https://www.ncei.noaa.gov/products/extended-reconstructed-sst.

**Acknowledgments**

This work was jointly supported by the National Natural Science Foundation of China (424B2035, U2442207), the Fundamental and Interdisciplinary Disciplines Breakthrough Plan of the Ministry of Education of China (JYB2025XDXM910), the Youth Innovation Promotion Association of Chinese Academy of Sciences (2021427), the West Light Foundation (xbzg-zdsys-202409) of the Chinese Academy of Sciences, and Central Guidance Fund for Local Science and Technology Development Projects in Gansu (No.24ZYQA031). We acknowledge the Computing Center in Xi'an for providing the computing resources.

## References

Aizen, E. M., Aizen, V. B., Melack, J. M., Nakamura, T., & Ohta, T. (2001). Precipitation and atmospheric circulation patterns at mid-latitudes of Asia. *International Journal of Climatology: A Journal of the Royal Meteorological Society*, *21*(5), 535–556. https://doi.org/10.1002/joc.626

Austin, P. C., & Tu, J. V. (2004). Bootstrap methods for developing predictive models. *The American Statistician*, *58*(2), 131–137. https://doi.org/10.1198/0003130043277

Barlow, M., Zaitchik, B., Paz, S., Black, E., Evans, J., & Hoell, A. (2016). A review of drought in the Middle East and southwest Asia. *Journal of Climate*, *29*, 8547–8574. https://doi.org/10.1175/JCLI-D-1300692.1

Chen, F., Huang, W., Jin, L., Chen, J., & Wang, J. (2011). Spatiotemporal precipitation variations in the arid Central Asia in the context of global warming. *Science China Earth Sciences*, *54*(12), 1812–1821. https://doi.org/10.1007/s11430-011-4333-8

Chen, F. H., Yu, Z. C., Yang, M. L., Ito, E., Wang, S. M., Madsen, D. B., et al. (2008). Holocene moisture evolution in arid central Asia and its out-of-phase relationship with Asian monsoon history. *Quaternary Science Reviews*, *27*(3–4), 351–364. https://doi.org/10.1016/j.quascirev.2007.10.017

Chen, X., Jia, X., Wu, R., & Qian, Q. (2022). Interannual variation and prediction of wintertime precipitation in Central Asia. *Journal of Climate*, *35*(14), 4771–4789. https://doi.org/10.1175/jcli-d-21-0951.1

Cheng, S., Yu, H., Zhou, J., Zhang, B., Ren, Y., Luo, H., et al. (2024). Impact of summer north Atlantic sea surface temperature tripole on precipitation over Mid–high-latitude eurasia. *Journal of Climate*, *37*(19), 5037–5053. https://doi.org/10.1175/jcli-d-24-0072.1

Deser, C., Phillips, A., Bourdette, V., & Teng, H. (2012). Uncertainty in climate change projections: The role of internal variability. *Climate Dynamics*, *38*(3–4), 527–546. https://doi.org/10.1007/s00382-010-0977-x

Donat, M. G., Lowry, A. L., Alexander, L. V., O'Gorman, P. A., & Maher, N. (2016). More extreme precipitation in the world's dry and wet regions. *Nature Climate Change*, *6*(5), 508–513. https://doi.org/10.1038/nclimate2941

Dong, W., Ming, Y., Deng, Y., & Shen, Z. (2024). Recent wetting trend over Taklamakan and Gobi Desert dominated by internal variability. *Nature Communications*, *15*(1), 4379. https://doi.org/10.1038/s41467-024-48743-x

Fallah, B., Didovets, I., Rostami, M., & Hamidi, M. (2024). Climate change impacts on Central Asia: Trends, extremes and future projections. *International Journal of Climatology*, *44*(10), 3191–3213. https://doi.org/10.1002/joc.8519

Fallah, B., & Rostami, M. (2024). Exploring the impact of the recent global warming on extreme weather events in Central Asia using the counterfactual climate data ATTRICI v1. 1. *Climatic Change*, *177*(5), 80. https://doi.org/10.1007/s10584-024-03743-0

Gerlitz, L., Steirou, E., Schneider, C., Moron, V., Vorogushyn, S., & Merz, B. (2018). Variability of the cold season climate in central Asia. Part I: Weather types and their tropical and extratropical drivers. *Journal of Climate*, *31*(18), 7185–7207. https://doi.org/10.1175/jcli-d-17-0715.1

Gerlitz, L., Steirou, E., Schneider, C., Moron, V., Vorogushyn, S., & Merz, B. (2019). Variability of the cold season climate in Central Asia. Part II: Hydroclimatic predictability. *Journal of Climate*, *32*(18), 6015–6033. https://doi.org/10.1175/jcli-d-18-0892.1

Guo, H., Tian, Y., Li, J., Meng, X., Lv, X., Wang, W., et al. (2024). Unveiling the spatiotemporal impacts of the 2021 Central Asian drought on vegetation: A comprehensive quantitative analysis. *Ecological Indicators*, *165*, 112238. https://doi.org/10.1016/j.ecolind.2024.112238

Guo, J., Xie, X., Myhre, G., Shindell, D., Kirkevåg, A., Iversen, T., et al. (2026). Distinct drivers of recent seasonal precipitation increase over Central Asia: Roles of anthropogenic aerosols and greenhouse gases. *Atmospheric Chemistry and Physics*, *26*(7), 5169–5184. https://doi.org/10.5194/acp-26-5169-2026

Held, I. M., & Soden, B. J. (2006). Robust responses of the hydrological cycle to global warming. *Journal of Climate*, *19*(21), 5686–5699. https://doi.org/10.1175/jcli3990.1

Hoell, A., Funk, C., & Barlow, M. (2015). The forcing of southwestern Asia teleconnections by low-frequency sea surface temperature variability during boreal winter. *Journal of Climate*, *28*(4), 1511–1526. https://doi.org/10.1175/jcli-d-14-00344.1

Huang, W., Chen, F., Feng, S., Chen, J., & Zhang, X. (2013). Interannual precipitation variations in the mid-latitude Asia and their association with large-scale atmospheric circulation. *Chinese Science Bulletin*, *58*(32), 3962–3968. https://doi.org/10.1007/s11434-013-5970-4

Huang, X., Zhou, T., Dai, A., Li, H., Li, C., Chen, X., et al. (2020). South Asian summer monsoon projections constrained by the interdecadal Pacific oscillation. *Science Advances*, *6*(11), eaay6546. https://doi.org/10.1126/sciadv.aay6546

Japan Meteorological Agency/Japan. (2013). JRA-55: Japanese 55-year Reanalysis, Monthly Means and Variances (updated irregularly) [Dataset]. *NSF National Center for Atmospheric Research*. https://doi.org/10.5065/D60G3H5B

Jiang, J., & Zhou, T. (2021). Human-induced rainfall reduction in drought-prone northern central Asia. *Geophysical Research Letters*, *48*(7), e2020GL092156. https://doi.org/10.1029/2020gl092156

Jiang, J., & Zhou, T. (2023). Agricultural drought over water-scarce Central Asia aggravated by internal climate variability. *Nature Geoscience*, *16*(2), 154–161. https://doi.org/10.1038/s41561-022-01111-0

Jiang, J., Zhou, T., Chen, X., & Wu, B. (2021). Central Asian precipitation shaped by the tropical Pacific decadal variability and the Atlantic multidecadal variability. *Journal of Climate*, *34*(18), 7541–7553. https://doi.org/10.1175/jcli-d-20-0905.1

Jiang, J., Zhou, T., Chen, X., & Zhang, L. (2020). Future changes in precipitation over Central Asia based on CMIP6 projections. *Environmental Research Letters*, *15*(5), 054009. https://doi.org/10.1088/1748-9326/ab7d03

Li, Y., Gong, H., Chen, W., & Wang, L. (2024). Attribution of drought trends on the Mongolian Plateau over the past decades. *Environmental Research Letters*, *19*(7), 074034. https://doi.org/10.1088/1748-9326/ad560d

Liu, Y., Cai, W., Zhang, Y., Lin, X., & Li, Z. (2024). Near-term projection of Amazon rainfall dominated by phase transition of the Interdecadal Pacific Oscillation. *npj Climate and Atmospheric Science*, *7*(1), 46. https://doi.org/10.1038/s41612-024-00587-4

Mariotti, A. (2007). How ENSO impacts precipitation in southwest central Asia. *Geophysical Research Letters*, *34*(16). https://doi.org/10.1029/2007gl030078

Monerie, P. A., Robson, J., Dong, B., & Hodson, D. (2021). Role of the Atlantic multidecadal variability in modulating East Asian climate. *Climate Dynamics*, *56*(1), 381–398. https://doi.org/10.1007/s00382-020-05477-y

Oki, T., & Kanae, S. (2006). Global hydrological cycles and world water resources. *Science*, *313*(5790), 1068–1072. https://doi.org/10.1126/science.1128845

Peng, D., Zhou, T., & Zhang, L. (2020). Moisture sources associated with precipitation during dry and wet seasons over Central Asia. *Journal of Climate*, *33*(24), 10755–10771. https://doi.org/10.1175/jcli-d-20-0029.1

Ren, Y., Yu, H., Huang, J., Zhou, J., Luo, H., & Cheng, S. (2025). Impact of mid-high latitude circulation and surface thermal forcing on drought events in central Asia. *Climate Dynamics*, *63*(2), 90. https://doi.org/10.1007/s00382-024-07577-5

Ren, Y., Yu, H., Liu, C., He, Y., Huang, J., Zhang, L., et al. (2022). Attribution of dry and wet climatic changes over Central Asia. *Journal of Climate*, *35*(5), 1399–1421. https://doi.org/10.1175/JCLI-D-21-0329.1

Rodgers, K. B., Lee, S. S., Rosenbloom, N., Timmermann, A., Danabasoglu, G., Deser, C., et al. (2021). Ubiquity of human-induced changes in climate variability. *Earth System Dynamics*, *12*(4), 1393–1411. https://doi.org/10.5194/esd-12-1393-2021

Schneider, U., Becker, A., Finger, P., Rustemeier, E., & Ziese, M. (2020). GPCC full data monthly product version 2020 at 0.5°: Monthly land-surface precipitation from rain-gauges built on GTS-based and historical data [Dataset]. https://doi.org/10.5676/DWD_GPCC/FD_M_V2020_050

Si, D., Hu, A., Meehl, G. A., Yu, L., Rosenbloom, N., & Jiang, D. (2025). Distinct roles of Atlantic multidecadal variability and external forcings on East Asian summer precipitation. *Journal of Climate*, *38*(22), 6493–6503. https://doi.org/10.1175/jcli-d-24-0695.1

Umirbekov, A., Peña-Guerrero, M. D., & Müller, D. (2022). Regionalization of climate teleconnections across Central Asian mountains improves the predictability of seasonal precipitation. *Environmental Research Letters*, *17*(5), 055002. https://doi.org/10.1088/1748-9326/ac6229

Wang, T., Xu, H., Jiang, D., & Yao, J. (2022). Mechanisms of reduced mid-holocene precipitation in arid central Asia as simulated by PMIP3/4 models. *Journal of Geophysical Research: Atmospheres*, *127*(8), e2021JD036153. https://doi.org/10.1029/2021JD036153

Wei, W., Zou, S., Duan, W., Chen, Y., Li, S., & Zhou, Y. (2023). Spatiotemporal variability in extreme precipitation and associated large-scale climate mechanisms in Central Asia from 1950 to 2019. *Journal of Hydrology*, *620*, 129417. https://doi.org/10.1016/j.jhydrol.2023.129417

Xie, T., Huang, W., Chang, S., Zheng, F., Chen, J., Chen, J., & Chen, F. (2021). Moisture sources of extreme precipitation events in arid Central Asia and their relationship with atmospheric circulation. *International Journal of Climatology*, *41*(S1), E271–E282. https://doi.org/10.1002/joc.6683

Yan, J., & Zhao, Y. (2022). Spatial evolution characteristics of precipitation and air temperature over central Asia. *Journal of Chengdu University of Information Technology*, *37*(5), 592–600. (In Chinese).

Yao, M., Tang, H., & Huang, G. (2024). Inter-model uncertainty in projecting precipitation changes over central Asia under global warming. *Geophysical Research Letters*, *51*(24), e2024GL111989. https://doi.org/10.1029/2024gl111989

Yao, M., Tang, H., Huang, G., & Wu, R. (2024). Interdecadal shifts of ENSO influences on Spring Central Asian precipitation. *npj Climate and Atmospheric Science*, *7*(1), 194. https://doi.org/10.1038/s41612-024-00742-x

Yao, M., Tang, H., & Huang, G. (2025). Roles of external forcing and internal variability in winter precipitation changes over Central Asia. *Earth's Future*, *13*, e2025EF006064. https://doi.org/10.1029/2025EF006064

Zhang, K., Zuo, Z., Suarez-Gutierrez, L., & Bu, L. (2024). The significant influence of the Atlantic multidecadal variability to the abrupt warming in Northeast Asia in the 1990s. *npj Climate and Atmospheric Science*, *7*(1), 28. https://doi.org/10.1038/s41612-024-00567-8

Zhang, W., Li, L., Zhou, T., Brody, M., He, Q., Xu, M., & Madibekov, A. (2025). Central Asian compound flooding in 2024 contributed by climate warming and interannual variability. *Advances in Atmospheric Sciences*, *42*(10), 1–8. https://doi.org/10.1007/s00376-025-4425-6

Zou, J., Ding, J., Welp, M., Huang, S., & Liu, B. (2020). Using MODIS data to analyse the ecosystem water use efficiency spatial-temporal variations across Central Asia from 2000 to 2014. *Environmental Research*, *182*, 108985. https://doi.org/10.1016/j.envres.2019.108985